Investigation of the densification mechanisms and corrosion resistance of amorphous silica films

Simon Ponton, Franck Dhainaut, Hugues Vergnes, Diane Samélor, Daniel Sadowski, Vincent R. Rouessac, Hélène Lecoq, Thierry Sauvage, Brigitte Caussat, Constantin Vahlas

Investigation of the densification mechanisms and corrosion resistance of amorphous silica films

Simon Ponton[a,b], Franck Dhainaut[a,b], Hugues Vergnes[b], Diane Samelor[a], Daniel Sadowski[a], Vincent Rouessac[c], Hélène Lecoq[d], Thierry Sauvage[d], Brigitte Caussat[b], Constantin Vahlas[a,*]

[a] CIRIMAT, Université de Toulouse, CNRS, Toulouse, France
[b] LGC, Université de Toulouse, CNRS, Toulouse, France
[c] IEM, Université de Montpellier, CNRS, ENSCM, Montpellier, France
[d] CEMHTI, CNRS, Orléans, France

ARTICLE INFO

Keywords:
Silica
TEOS
CVD
Densification
FTIR
P-etch test

ABSTRACT

The barrier properties of the technologically attractive amorphous silica films depend on their structural characteristics at the atomic level, which, in turn are strongly influenced by the deposition conditions. In this paper, we propose an investigation of the poorly investigated densification mechanism of amorphous SiO_2 films processed by CVD from TEOS and O_2 between 400 and 550 °C. Based on literature survey and our original experimental results, we show that the densification process of these films, occurring with increasing the deposition temperature, is highlighted by a decrease of the water and silanol content, probed by transmission FTIR. We discuss the evolution of Si-O-Si related vibration signatures and we use the central force model to correlate the LO_2 and LO_3 shifts with the decrease of the Si-O-Si bond force constant, when the deposition temperature increases. Nuclear analysis reveals that films processed below 525 °C present hydrogen content between 5 ± 0.3 and 7 ± 0.3%at. Ellipsometry measurements attest that films processed at 550 °C are close to O/Si silica stoichiometry and hydrogen free. We show that application of the P-etch test results in particularly low erosion rate of 10 Å.s^{-1} for dense films processed at 550 °C.

1. Introduction

Thin and dense SiO_2 films processed from tetraethyl orthosilicate (Si$(OC_2H_5)_4$, TEOS) by chemical vapor deposition (CVD) have long been considered to solve mainly microelectronic issues, such as copper diffusion barrier, dielectric capacitor and intermetallic dielectric layers for multilayer metallization systems [1]. Nowadays, such films remain key enabling materials in innovative applications and devices [2–6]. These applications have in common a low thermal budget process requirement due to thermally sensitive, or 3D complex geometry substrates. Addition of oxygen [7] or ozone O_3 [8] in the gas phase or the use of plasma assistance (PECVD) [9,10] are well known actions resulting in lower thermal budget processes, yielding silica films at moderate temperatures, typically lower than 600 °C. More recently, atomic layer deposition (ALD) of SiO_2 thin films has also been performed at low temperature to solve optical applications issues [11] or to cap nanoporous anodic alumina membranes employed in biosensor devices [12]. The correlation between the effects of such low temperature deposition and the atomic arrangement of the silica structure is not well understood, especially considering that the densification process is complex and multi parameter dependent [13]. However, the atomic arrangement of the material is the key to understand its targeted barrier properties when such silica films are used as barrier coatings [4,5] or to understand the special selectivity of gases when it is used in gas membranes [6].

The structure of the amorphous SiO_2 films has been defined by Sen and Thorpe [14] and Galeener [15] as a short range organized continuum built up from tetrahedral entities centered on a silicon atom. Each oxygen atom at the corner of a tetrahedron is shared by another tetrahedral unit and cross links the entire network. Twofold coordinated bridging oxygen is more mobile than fourfold coordinated silicon and has been considered as the main contributor to the atomic vibration of this system [16]. Vibration modes of this oxygen are intimately related to the SiO_2 structure and, consequently, the spectral changes under densification should reveal information on the atomic distribution of the network. Three vibration modes of the oxygen atom linked with two silicon atoms are assigned in the mid infrared (IR) region between 400 cm^{-1} and 4000 cm^{-1}. These are the transversal

* Corresponding author.
E-mail address: constantin.vahlas@ensiacet.fr (C. Vahlas).

optical rocking (TO_1), bending (TO_2) and asymmetric stretching (TO_3) modes, which are observed respectively at around 450 cm^{-1}, 800 cm^{-1} and 1070 cm^{-1} [16]. The TO_1 mode is sensitive to structural changes [17] but its frequency shift is too weak to be monitored by FTIR, i.e. the shift is in the same order of magnitude with the measurement uncertainties. An additional vibration mode, the TO_4, is assumed by some authors between 1050 cm^{-1} and 1250 cm^{-1} [18–20]. It has been attributed to the out of phase vibrations of the TO_3 mode [20,21], to the longitudinal, LO_3 mode in this area [22], to the presence of residual TEOS molecules [23] and to strained 3 to 6 fold Si—O rings [19,24,25]. The debate around the attribution of a physical phenomenon to the TO_4 broad band reveals the difficulty to correlate the existence and the characteristics of this vibration with the short range organization of the network. This difficulty may be attributed to the intrinsic nature of the material, which is amorphous, with randomly crosslinked tetrahedral entities [15]. Thus, the overall characteristics of CVD SiO_2 films, such as stoichiometry [26,27], porosity [28], impurities [29,30] and mechanical strain [24] which depend on the process conditions, will affect the FTIR signature, the evolution of the refractive index and consequently they may bias the interpretation of the densification process.

This literature review reveals that, despite uncertainties on the origin of some vibrations, FTIR is an appropriate technique to monitor the evolution of the silica network, and for this reason it will be used in the present work. We will adopt the central force model proposed by Sen and Thorpe [14] and applied to glasses by Galeener [15] in order to link FTIR signatures to structural changes. This model connects SiO_2 vibrations to the Si O Si intertetrahedral bond angle, θ, and the Si—O force constant, α, of the SiO_2 network [31]. Nonetheless, the model assumes perfect stoichiometric, continuous SiO_2 network and it takes into account neither composition deviations, namely the offset with regard to the nominal O/Si ratio, nor the presence of heteroatoms such as carbon impurities, nor the porosity, nor the mechanical strain that can be observed in CVD SiO_2 films. Consequently, and in order to elaborate a scenario of the evolution of the structure under different process temperatures (T_d), we perform complementary characterizations to get insight on these parameters: we quantify by nuclear analysis the concentrations of silicon, oxygen and hydrogen; we determine both the refractive index by reflection spectroscopic ellipsometry (SE) using the Sellmeier model, and the porosity by ellipsometric porosimetry (EP) measurements using the Cauchy model. Finally, we apply selective chemical corrosion tests proposed by Pliskin [13,32] in order to correlate the evolution of the structure with its intrinsic resistance towards aggressive medium.

2. Experimental

Depositions were performed in a horizontal, hot wall tubular CVD reactor, presented in the supplementary material (Fig. S1). For each experiment, six $30 \times 10 \times 0.2\,mm^3$ Si coupons cut from 4' Si(100) wafers (Sil'tronix ST) were degreased in sequential acetone and ethanol ultrasound baths for 5 min each, dried in Ar flow, positioned on a stainless steel planar substrate holder and immediately introduced in the reactor. TEOS vapors were introduced in the reactor by bubbling 58 standard cubic centimeters (sccm) of nitrogen, N_2 (99.9999%, Messer) though the liquid precursor heated at 51 °C. 520 sccm of O_2 (99.999%, Messer) are added to the mixture just before the reaction chamber. Experiments were performed at five different T_d, namely 400 °C, 450 °C, 500 °C, 525 °C and 550 °C, at a constant pressure of 730 Torr. An annealing at 800 °C during 30 min under ambient atmosphere was performed on one sample processed at 550 °C. The thickness profiles of the SiO_2 films on all coupons were measured by reflectometry and served to deduce mechanistic and kinetic information for each experimental condition. More information about the deposition setup and the kinetic results obtained is available in our recent companion paper which deals with the development of a kinetic model of this process [7].

FTIR spectrometry was performed in transmission mode with a Frontier FT IR/NIR instrument. The 400–4000 cm^{-1} spectral range was probed with a 2 cm^{-1} spectral resolution. Fifty spectrum accumulations were performed for each experiment. Raw data were processed in order to remove light interferences and substrate signature. The position of SiO_2 peaks are affected by the thickness of the film in transmission mode [33]. Films with similar thicknesses were investigated, ranging from 338 nm to 416 nm and the absorbance was normalized by the film thickness. A homemade substrate holder was used in order to apply an angle between the incident beam and the sample, to observe the TO LO splitting.

Two instruments were used for ellipsometry investigations. First, EP measurements were used to evaluate the open nanoporosity of the films. A Semilab GES5E spectroscopic ellipsometer was used on pur pose, operating between 250 nm and 1000 nm, at a fixed incidence angle of 70°. This ellipsometer is completed with a lab made chamber set up for automatic vapor adsorption desorption investigation [34,35]. Porosity was estimated by probing the evolution of the refractive index due to the intake of the ethanol by the structure. Before any acquisition of the refractive index and thickness of the layer, the sample was maintained under vacuum at 150 °C to desorb water or other volatile adsorbed compounds. Refractive index and thickness calculation were monitored at variable ethanol pressures by adding gradually the solvent in the chamber. The filled pore fraction of the open pores is a function of the partial pressure of the solvent above the sample. Ellipsometric data tan(psy) and cos(delta) are collected then simulated and fitted on the 390–1000 nm spectral range with a goodness of fit over 0.99, using the Cauchy model (Winelli2® software).

In addition, a Semilab SE 2000 instrument operating in the 250 nm to 1000 nm spectral range with fixed incidence angle of 70° was used to evaluate the refractive index by SE. The spectroscopic ellipsometry data were simulated and fitted using the Semilab SEA software. The Sellmeier model was used as a reference to determine the refractive index and the films thickness.

The O/Si atomic ratio of film was determined by coupling the Rutherford Backscattering Spectroscopy (RBS) and Nuclear Reaction Analysis (NRA) techniques for Si and O analysis, respectively. RBS was performed at a 166° detection angle with 2 MeV α particles. The oxygen concentration was measured through the use of the $^{16}O(d,\alpha_0)$ nuclear reaction with D^+ ion beam of energy 0,9 MeV and at a 166° detection angle of emitted alphas. The hydrogen content of SiO_2 film was measured by ERDA with 2,8 MeV alphas beam. The samples were positioned at 15° grazing incidence and the recoiled hydrogen atoms were collected at scattering angle of 30°. The global composition of films is obtained through the simulation of the RBS, NRA and ERDA spectra by using the SIMNRA software [36].

The corrosion resistance of the films was evaluated by using the P etch solution test, proposed by Pliskin [13]. The test consists in immerging the sample for 30 s in a stirred solution maintained at 25 °C. The solution is composed of 3 parts hydrofluoric acid (49 wt%), 2 parts of nitric acid (70 wt%), and 60 parts of water. The P etching rate for each sample corresponds to the thickness loss for a given etching time, determined by SE and is given in $Å.s^{-1}$,

3. Results and discussion

3.1. FTIR

Fig. 1 presents a typical 400–4000 cm^{-1} FTIR survey spectrum of a SiO_2 film processed at T_d = 400 °C. According to the literature [16], the TO_1, TO_2 and TO_3 vibration modes are detected at 450 cm^{-1}, 798 cm^{-1} and 1074 cm^{-1}, respectively. The TO_4 broad band appears around 1100–1200 cm^{-1}. Water content is observed between 3300 and 3600 cm^{-1} and silanol fingerprints are probed at 925 cm^{-1} and 3650 cm^{-1}. Neither carbon (Si—C) [37] nor CH_3 [38] nor Si—H impurities related vibrations [29,39–41], expected respectively at 600, 1300 and 2000 cm^{-1}, are present.

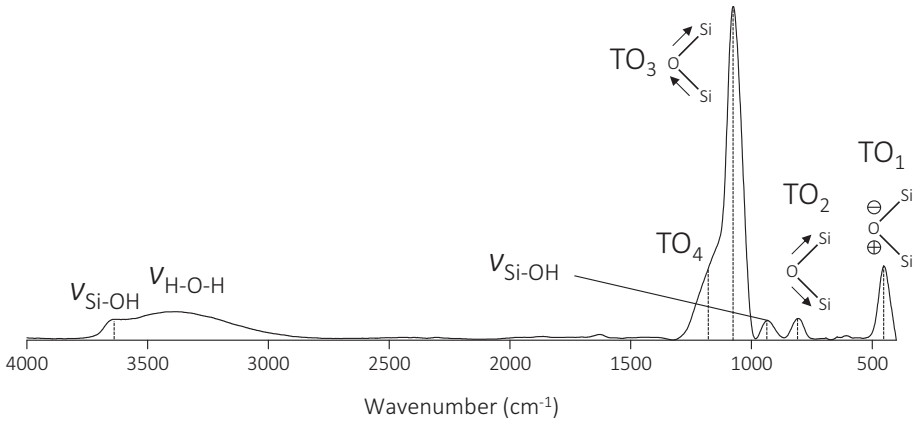

Fig. 1. FTIR survey spectrum of a SiO_2 film processed at T_d = 400 °C.

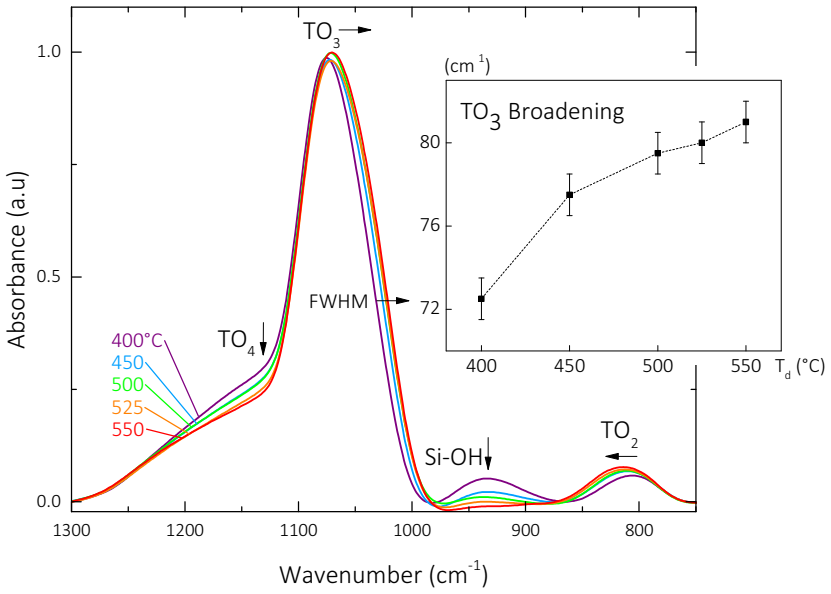

Fig. 2. Zoom in the 700–1300 cm^{-1} zone of the FTIR spectra containing the Si-OH, TO_2, TO_3, TO_4 vibrational modes, and their evolution as a function of T_d. The evolution of the TO_3 peak broadening is plotted as a function of T_d.

Fig. 2 presents a zoom on the 700 1300 cm^{-1} region of the FTIR spectrum of five samples processed at different T_d, from 400 °C to 550 °C. This spectral domain includes the Si OH, and SiO_2 vibrations modes (TO_2, TO_3 and TO_4). A color code is applied for each T_d and it will be used in all forthcoming illustrations. Several informations are highlighted in this figure. First, a slight, though noticeable evolution of the position of the TO_3 peak, corresponding to the asymmetric stretching vibration mode is observed with increasing T_d. At the same time, the TO_3 peak broadens, from 72.5 cm^{-1} at 400 °C to 81 cm^{-1} at 550 °C as shown by the diagram in the insert of Fig. 2. Finally, a de crease of Si OH intensity is observed when T_d increases. These three informations will be discussed hereafter in other to have an insight into the reorganization of silica films when T_d increases.

3.1.1. Evolution of TO_3 frequency with the increase of T_d

It has been reported that the information contained in the evolution of the position of the TO_3 peak, provides insight in the densification process of the SiO_2 network [13,42]. According to these authors, the shift to higher wavenumbers (blue shift) of the TO_3 peak position in dicates the densification of the SiO_2 network and conversely, a shift to lower wavenumbers (red shift) is assigned to a decrease of the density.

Fig. 3 presents the evolution of the position of the TO_3 peak as a function of T_d of the CVD samples of the present work (mauve diamond plots). The point at the highest temperature corresponds to a sample deposited at 550 °C and annealed at 800 °C for 30 min. We observe a red shift of the TO_3 peak position with increasing T_d, while the peak po sition of the annealed sample shifts to a higher value. For sake of comparison, a compilation of literature data is also reported in Fig. 3, as a function of deposition or post deposition annealing temperature [23,43 49]. Empty symbols correspond to sol gel, room temperature processed, then annealed SiO_2 films. Full symbols correspond to plasma enhanced CVD (PECVD) SiO_2 films, processed between room tem perature and 250 °C. Two regimes are illustrated in the diagram. For deposition, or post deposition annealing temperatures equal to, or lower than 600 °C, the TO_3 position presents a red shift or remains stable with increasing temperature. Above 600 °C, it presents a blue shift with increasing temperature.

Literature and our own data present a remarkable coherence. The global behavior of all chemical systems used for the processing of SiO_2 films indicates that the assumption following which densification is illustrated by a blue TO_3 shift, is not relevant for films processed and/or annealed below 600 °C. This inconsistency is attributed to films defects such as porosity, impurities or mechanical strain resulting in less dense organization of the tetrahedral network [13]. The previously described TO_4 broad band is the representation of the disorder of the network and it is relatively high for every silica films processed at temperature lower

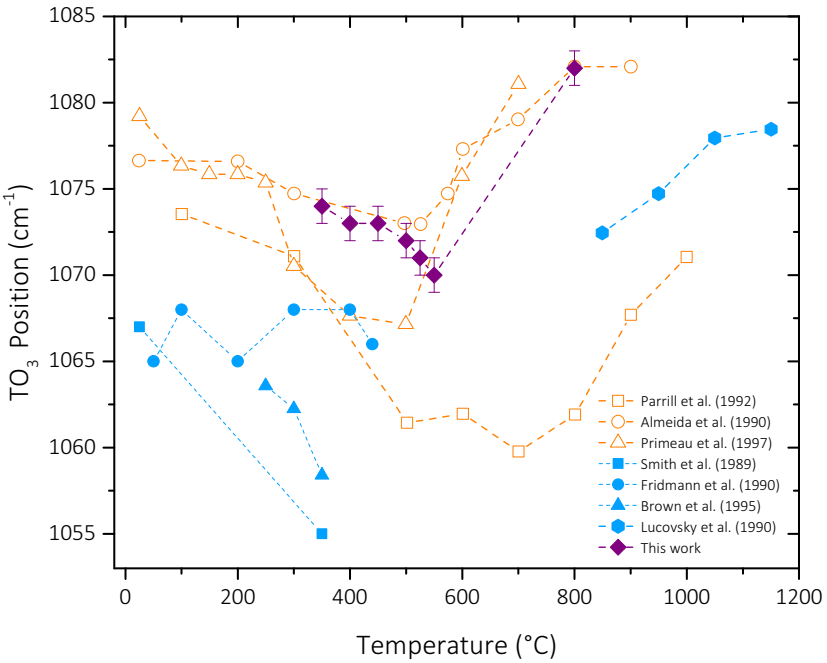

Fig. 3. Overview of TO_3 position as a function of post-annealing temperature for SiO_2 films. Empty symbol data: sol-gel films processed at room temperature. Full symbol data: PECVD films processed between room temperature and 250 °C. Empty squares [25], empty dots [43], empty triangles [23], full squares [48], full dots [49], full triangles [46], full pentagons [44]. Full diamonds correspond to samples of the present work positioned as a function of the deposition temperature. The point at the highest temperature corresponds to a sample deposited at 550 °C and annealed at 800 °C for 30 min.

than 600 °C. This peak can strongly impact the position of the TO_3 peak. At and above 600 °C, the Si O Si asymmetric stretching vibration mode is less impacted by the TO_4 broad band because fewer defects might be observed in the structure. Consequently, the TO_3 peak position presents a blue shift with increasing temperature [44].

3.1.2. *Broadening of TO_3 peak with the increase of T_d*

The broadening of the TO_3 peak revealed in Fig. 2 was also observed for PECVD SiO_2 films [48]. This behavior is attributed to a dis organization of the network [50] and thus it cannot be linked to the densification of the SiO_2 structure, either. Nonetheless, a close ob servation reveals that this broadening is not related to the increase of the full width at half maximum (FWHM) of the peak but rather to a change in its shape. At high T_d, the peak can no longer be fitted by only one gaussian or lorentzian function. The peak is shifted due to the asymmetric, one side increase of the peak area. An addition of a second contribution had to be assumed. The existence of two contributions below the TO_3 main peak has been already suggests by authors [51,52]. To explain this behavior, they assigned the contribution of two asym metric stretching mode vibrations from two different phases.

3.1.3. *Decrease of hydrated species specific peak intensities with the increase of T_d*

Fig. 2 reveals a simultaneous decrease of the intensities of the TO_4 vibration shoulder and of the Si OH vibrations located at 925 and 3650 cm^{-1} with increasing T_d. Above T_d = 500 °C, almost no Si OH located at 925 cm^{-1} is probed. In order to confirm this trend, it is useful to focus on the 2750 3800 cm^{-1} spectral domain, also containing Si OH and H OH vibrations. Fig. 4 presents the FTIR spectra in this do main for the samples processed in the five investigated T_d. A common baseline has been adopted for all five spectra. The insert in Fig. 4 presents the evolution, with increasing T_d, of the peak intensities of the Si OH and H OH vibrations located at 3650 cm^{-1} and at 3400 cm^{-1}, respectively. As is the case for the Si OH vibrations located at 925 cm^{-1}, their intensity in the presented spectral domain also de creases with increasing T_d, and the same holds for the H OH vibration. Moreover, it is observed in the insert of the figure that this decrease is slightly accelerated above 500 °C for both bonds.

When T_d increases, the structure is less hydrated as shown from the decrease of the H_2O and Si OH vibrations in Fig. 4. At the same time, the intensity of TO_4 decreases and the TO_3 peak area increases. More over, the attenuation of the TO_3 broadening above 450 °C observed in Fig. 2, can be correlated to the reduced Si OH population above this temperature. Based on this assumption, we suggest that at moderate temperature; i.e. below 600 °C, the SiO_2 network is composed of cross linked Si O Si units with impurities which impact Si—O—Si asymmetric stretching "out of plane" mode vibrations (TO_4 shoulder) [19,23,24]. These impurities can be assigned to hydrogen species (H_2O and Si OH) or structural disorder such as space among SiO_4 tetrahedra [53]. At higher temperature, additional Si O Si bonds are created and the amount of impurities decreases. This scenario results in the presence of two populations of Si O Si bonds, the classic Si O Si bond population which vibrates at the TO_3 vibration frequency and another one re presented by the TO_4 vibration mode or by another asymmetric vi bration mode suggested by authors [51,52]. Si O Si groups that vibrate at the TO_4 frequency are the one impacted by impurities [23] or por osities [19,24]. As soon as the signature of hydrogen species decreases when Td increases, TO_4 decreases and the position and shape of the TO_3 change as described. In order to check this assumption and to link the FTIR signature to structural changes, it is essential to further investigate the deconvolution of each contribution, especially in the TO_3 TO_4 re gion.

3.1.4. *TO_3 LO_3 splitting*

By applying an oblique incidence of the infrared beam on the sample, the interaction of the electromagnetic field with the film is enhanced and the asymmetric stretching mode is split into two com ponents [54], the transverse optical excitation (TO) and the long itudinal optical one (LO), the latter called the Berreman effect [55,56]. Fig. 5 presents the evolution of each component of the asymmetric stretching mode for the five T_d, for an incidence angle of 60° with the sample surface. A similar behavior to the one described hereafter is observed for all other tilt angles. The shape of the TO_3 peak varies when tilted, with non Gaussian type evolution when T_d increases, as pre viously reported. This is attributed to the existence of two populations of the Si O Si group. At the same time, the TO_3 position presents a red shift, while the position of the longitudinal component (LO_3) presents a blue shift. Similar observations were obtained on mesoporous SiO_2 films [57]. Due to TO_4 splitting, Lange et al. [54] attributed TO_4 and LO_4 frequencies at 1200 cm^{-1} and 1170 cm^{-1} respectively. While TO_3

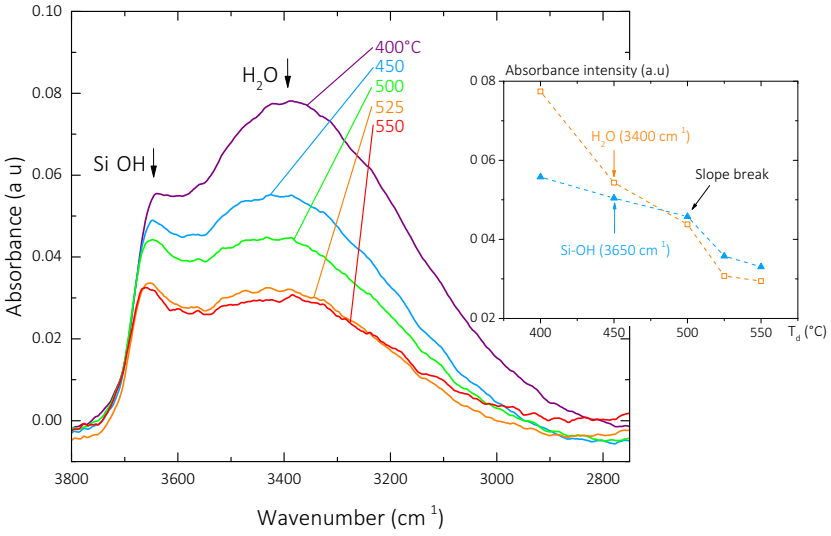

Fig. 4. Zoom in the 2750–3800 cm^{-1} zone of the FTIR spectra containing Si-OH and H_2O vibrational modes, for films processed at different T_d. Insert: Evolution of the absorbance intensity of H_2O and Si-OH peaks as a function of T_d.

and LO_3 probe the same asymmetric stretching vibration mode, other types of vibration may less bias the LO_3 response. Consequently, the blue shift observed for the LO_3 peak is predominantly attributed to the asymmetric stretching vibration [58,54].

In order to confirm the effective densification of the SiO_2 network with increasing T_d, as assumed by the blue shift of LO_3, we now apply the central force model which correlates the different Si O Si vibration frequencies (ω, cm^{-1}) with the effective force constant (α, $N.m^{-1}$) and the angle (θ) of the bond [15]:

$$\alpha = \tfrac{1}{2}(\omega_{LO2}{}^2 + \omega_{LO3}{}^2)\, M_O (1 + 4M_O/3M_{Si})^{-1} \quad (1a)$$

$$\cos\,\theta = (\omega_{LO2}{}^2 - \omega_{LO3}{}^2)\,(\omega_{LO2}{}^2 + \omega_{LO3}{}^2)^{-1}(1 + 4M_O/3M_{Si}) \quad (1b)$$

where M_O (16 $g.mol^{-1}$) and M_{Si} (28 $g.mol^{-1}$) are the molar masses of oxygen and silicon. The evolution of the effective force constant and of the angle of the Si O Si bond versus T_d can be determined by mea suring the evolution of the LO_2 and LO_3 frequencies, ω_{LO2} and ω_{LO3}. Since the TO_2 LO_2 splitting is negligible, TO_2 and LO_2 frequencies are merged and the evolution of the LO_2 frequency is assumed identical to that of the TO_2 one. Table 1 details the LO_2 and LO_3 shifts, the evolu tions of the force constant and of the intertetrahedral bond angle as a function of T_d. The model predicts that with increasing T_d, the effective force constant increases and the intertetrahedral bond angle remains stable. It is concluded that, by differentiating the TO_3 LO_3 pairs, it is possible to isolate the asymmetric stretching contribution and to con firm the densification of the SiO_2 network, despite the red shift which is observed for the TO_3 peak.

Table 1
TO_2 and TO_3 peak shifts, effective force constant (α) and angle (θ) versus T_d.

T_d (°C)	ω_{LO2} (cm^{-1})	ω_{LO3} (cm^{-1})	α ($N.m^{-1}$)	θ (°)
400	798	1231	570.2	134.8
450	806	1232	572.1	134.4
500	809	1234	574.2	134.3
525	811	1235	575.7	134.1
550	813	1238	578.1	134.3

3.2. *Nuclear analysis*

The red shift of the TO_3 vibration mode is assigned to films defects in general, including impurities. We perform ion beam analysis in order to access the composition of the films processed between 400 °C and 550 °C. The results are resumed in Fig. 6 in terms of the evolution of the O/Si atomic ratio and of the atomic percentage of hydrogen atoms as a function of T_d.

Between 400 and 525 °C the O/Si atomic ratio remains stable at a value slightly higher than 2, attributed to the presence of H_2O

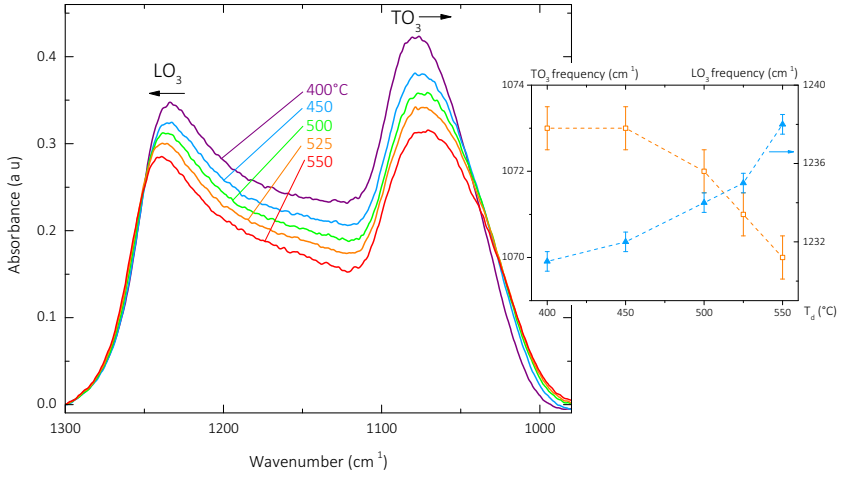

Fig. 5. Zoom in the 1000–1300 cm^{-1} zone of the FTIR spectra, obtained for a 60° tilt of the incident beam with the sample surface, of SiO_2 films processed at different T_d. The two TO_3 and LO_3 peaks are obtained from the split of the asymmetric stretching mode in these probing conditions. Insert: Shift of the TO_3 and LO_3 peaks as a function of T_d.

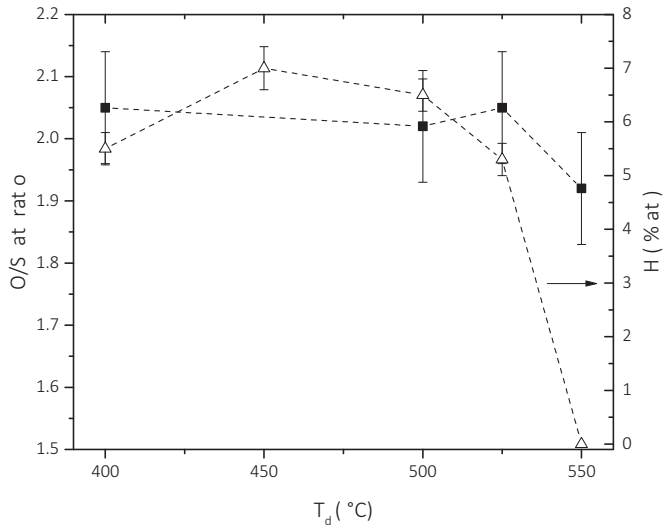

Fig. 6. Evolution of the O/Si atomic ratio (filled squares) and of the atomic percentage of hydrogen atoms (open triangles) as a function of T_d, probed by ion beam analysis. Dotted lines are guide to the eye.

molecules in the network as was revealed by FTIR. This ratio decreases to ca. 1.93 at 550 °C. However, this evolution remains within the uncertainty of the measurements. At T_d equal to or lower than 525 °C, the hydrogen concentration varies between 5.0 ± 0.3 and 7.0 ± 0.3 at.%. At T_d = 550 °C, it is below the detection limit of ERDA, namely 0.5 at.%. These results are consistent with a decrease of the concentrations of water and silanol groups at 550 °C. Silanol groups were not probed at 925 cm^{-1} by FTIR at this temperature and a low signal was probed for water and silanol groups at 3650 cm^{-1}. However, the decrease of water content and silanol groups between 400 and 525 °C, observed by FTIR, is not probed by nuclear analysis. This can be attributed to the conditioning of the samples under secondary vacuum during nuclear analysis, resulting to water desorption from the structure. It can also be attributed to the current density received by the sample under the ion beam which may result in a preferential desorption.

It is worth noting that hydrogen containing silica films have often been reported in the literature. For example, films processed by plasma enhanced ALD and thermal, ozone involving ALD from various silicon precursors present a relatively high hydrogen concentration, in the range 10 to 13 at.% [59]. Also, films processed by PECVD from hexamethyldisiloxane (HDMSO) and O_2 present a T_d dependent hydrogen concentration, decreasing from 18.5 at.% at 50 °C to 5.3 at.% at 300 °C [60].

The significant amount of hydrogen probed by nuclear analysis and a non negligible amount of water probed by FTIR can be assigned to the deposition process since it is a by product of the CVD reaction between TEOS and oxygen [61]. It can also be due to the post processing adsorption of water in the SiO_2 structure, as reported by some authors [62 64]. For example, Lucovsky et al. observed a significant intake of H_2O after 5 days storage at ambient atmosphere which has a strong effect into the TO_3 band [64].

Also, thermal desorption and FTIR studies of the gas evolution and the microstructure of PECVD silicon oxide grown between 70 and 700 °C from TEOS and oxygens show that between 100 and 300 °C, gas desorption is due to adsorbed water in the film during air exposure, originating from liquid water and hydrogen bonded water molecules at the macropore site [65]. At higher temperature, from 350 °C to 650 °C, gas desorption is related to the isolated silanol bonds at the macro and micropore sites formed during film growth.

3.3. Ellipsometry

The densification of the films involves an evolution of their porosity, taken in the broader sense of the free space available among the SiO_4 tetrahedra. In order to get insight in this parameter, two films processed at 400 and at 550 °C; i.e. the highest and lowest T_d were characterized by EP. The refractive index, n_{550}, of the film processed at 550 °C, determined using the Cauchy model, was shifted from 1.450 to 1.423 after the warm up stage up to 150 °C. Taking into account that this temperature is too low to induce structural modifications in the film, the evolution of the refractive index gap can be assigned to water removal, contained in the film ($n_{void} = 1 < n_{H2O}$). Then, ethanol was introduced in the chamber. The value of n_{550} remained unchanged to 1.423. EP measurements were not sensitive enough to determine a possible porosity in the films. In the literature, ultra microporous SiO_2 films exhibit a porosity smaller than 1 nm [66]. Studies were done in order to understand the adsorption of water molecules inside 1.04, 1.96 and 2.88 nm diameter silica pores [67]. The proposed scenario considers the coverage of the surface of each pore by silanol groups. A first stage, defined by a preferential adsorption of the water molecule near silanol groups, is followed by the formation of a water monolayer over the entire pore surface. In the presence of excess water molecules, pores are completely filled with water.

The evolution of the refractive index versus T_d using the Sellmeier models is presented in Fig. 7. Two regimes are observed; below T_d = 500 °C the refractive index remains stable. Above 500 °C, the refractive index decreases. Two scenarios are reported in the literature for the correlation between the characteristics of the SiO_2 films and their refractive index: for stoichiometric films, the refractive index increases when the network becomes denser due to the decrease of porosity content that contain void or water with a refractive index of the environment lower than that of SiO_2 [68]. For non stoichiometric SiO_x films, the refractive index decreases when the SiO_2 network becomes denser [69]. This behavior is assigned to the incorporation of oxygen in the structure, this enrichment goes with a decrease of the refractive index because $n_{Si} > n_{SiO} > n_{SiO2}$.

At T_d up to 500 °C, the stability of the refractive index can be attributed to a film composition that remains stable as suggested by nuclear analysis. However, this conclusion does not fit FTIR results, which reveal a decrease of the H_2O and Si OH FTIR vibration modes when T_d increases. To counterbalance the expected decrease of the refractive index due to the dehydration of the layer, the incorporation of oxygen

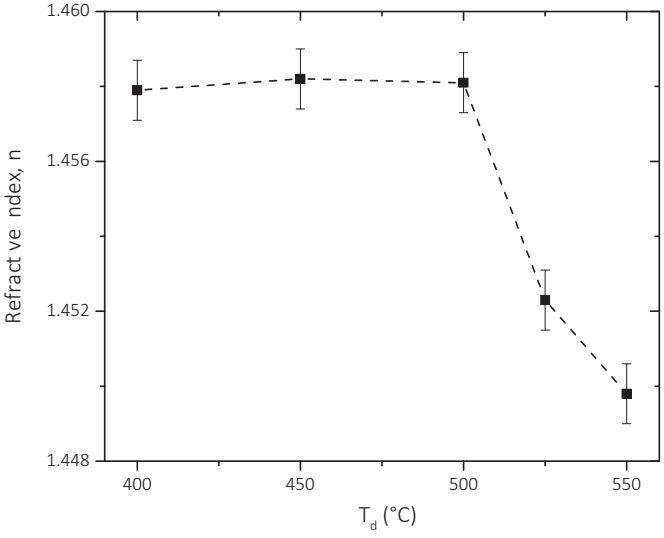

Fig. 7. Evolution of the refractive index of the SiO_2 films processed between 400 °C and 550 °C determined by the Sellmeier model.

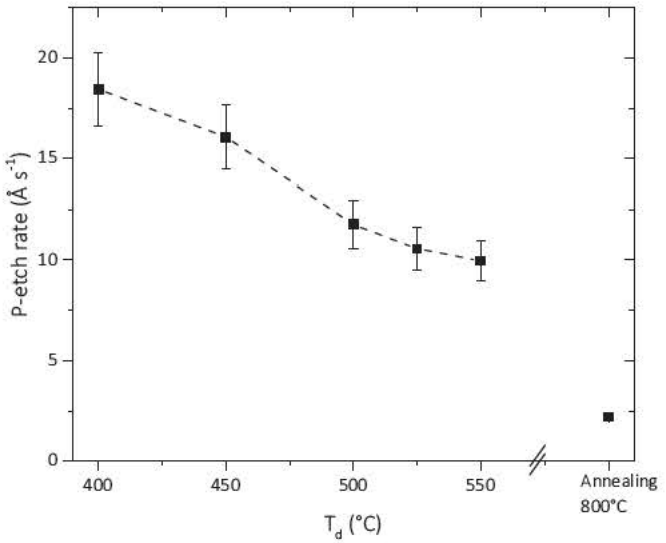

Fig. 8. P-etch rate versus T_d and post-annealing at 800 °C for the SiO_2 films.

in the network is considered when T_d increases above 500 °C. At this temperature range, the incorporation of oxygen can indeed be assigned to the generation of new Si O Si bonds. This result suggests an increase of the structure densification when T_d increases.

3.4. Corrosion resistance

Pliskin proposed in 1964 an etching solution in order to comparatively investigate the resistance of various glass and oxide film systems [32]. Since then, the Pliskin etch or P etch has been commonly adopted in order evaluate the impact of the type of deposition technique, of the chemistry and of the different process parameters on the resistance to the involved corrosive solution of the SiO_2 films. Fig. 8 presents the P etch rate ($Å.s^{-1}$) of the films deposited between 400 °C and 550 °C. The resistance to the corrosive solution is clearly improved with increasing T_d, from 18 $Å.s^{-1}$ to 10 $Å.s^{-1}$. These results favorably compare with those of previously reported SiO_2 films processed below 600 °C by PECVD [70] or using ozone [71], for which the P etch rate varies between 8 and 53 $Å.s^{-1}$. An annealing at 800 °C during 30 min of the films (independently of T_d) presents a P etch rate of 2 $Å.s^{-1}$; i.e. similar to the denser silica film obtained by pyrolysis at temperature higher than 975 °C [13]. This behavior is indirectly linked to the porosity, the composition, the stoichiometry and ultimately to the density of the films [13].

4. Conclusions

An original methodology is developed in order to propose a comprehensive scenario for the densification mechanism of CVD SiO_2 films processed from TEOS and oxygen in the temperature range 400 550 °C. The combination of different characterization techniques allows assigning the densification process first to a dehydration of the film based on the decrease of the water and silanol peaks, revealed by FTIR. A significant hydrogen content between 5 ± 0.3%at. and 7 ± 0.3%at. is determined by nuclear analysis for films processed below T_d = 525 °C. Films processed at T_d = 550 °C are hydrogen free and present a slightly substoichiometric structure. Ellipsometric porosimetry allows concluding that if the films present porosity, the diameter of this porosity might be smaller than the detection limit of EP measurements. The corrosion resistance, probed by the P etch rate test, is improved from 18 to 10 $Å.s^{-1}$ with increasing T_d; i.e. with the Si—O—Si network densification. Upon annealing at 800 °C for 30 min, the P etch rate is further improved, decreasing to 2 $Å.s^{-1}$, the lowest reported value for SiO_2, similar to the one of films obtained from the pyrolysis of TEOS at almost 1000 °C. This test indirectly confirms the densification of the film with increasing T_d. The integration of the reported various experimental information confirms the proposed mechanism and indicates that amorphous SiO_2 films processed from TEOS and oxygen at 550 °C, are dense and thus present high normalized corrosion resistance.

Acknowledgments

We are indebted to Olivier Debieu, CIRIMAT Toulouse for advice with the ellipsometry investigations, and to Benoit Ridard and Hervé Guegan, ARCANE CENG Bordeaux for the nuclear investigations. This work was partly supported by the Agence Nationale de la Recherche (ANR) under contract #ANR 17 CE08 0056.

References

[1] S.P. Murarka, R.J. Gutmann, A.E. Kaloyeros, W.A. Lanford, Advanced multilayer metallization schemes with copper as interconnection metal, Thin Solid Films 236 (1993) 257–266, https://doi.org/10.1016/0040-6090(93)90680-N.
[2] S. Callard, A. Gagnaire, J. Joseph, New method for in situ control of Bragg reflector fabrication, Appl. Phys. Lett. 68 (1996) 2335–2336, https://doi.org/10.1063/1.115849.
[3] C. Martinet, V. Paillard, A. Gagnaire, J. Joseph, Deposition of SiO2 and TiO2 thin films by plasma enhanced chemical vapor deposition for antireflection coating, J. Non-Cryst. Solids 216 (1997) 77–82.
[4] A.G. Erlat, B.-C. Wang, R.J. Spontak, Y. Tropsha, K.D. Mar, D.B. Montgomery, E.A. Vogler, Morphology and gas barrier properties of thin SiOx coatings on polycarbonate: correlations with plasma-enhanced chemical vapor deposition conditions, J. Mater. Res. Pittsburgh 15 (2000) 704–717, https://doi.org/10.1557/JMR.2000.0103.
[5] P.A. Premkumar, S.A. Starostin, M. Creatore, H. De Vries, R.M.J. Paffen, P.M. Koenraad, P.A. Premkumar, M.C.M. Van De Sanden, S.A. Starostin, Smooth and self-similar SiO2-like films on polymers synthesized in roll-to-roll atmospheric pressure-PECVD for gas diffusion barrier applications, Plasma Process. Polym. 7 (2010) 635–639, https://doi.org/10.1002/ppap.200900179.
[6] S. Nitodas, E. Favvas, G. Romanos, M. Papadopoulou, A. Mitropoulos, N. Kanellopoulos, Development and characterization of silica-based membranes for hydrogen separation, J. Porous. Mater. 15 (2008) 551–557, https://doi.org/10.1007/s10934-007-9132-4.
[7] S. Ponton, H. Vergnes, D. Samelor, D. Sadowski, C. Vahlas, B. Caussat, Development of a kinetic model for the moderate temperature chemical vapor deposition of SiO2 films from tetraethyl orthosilicate and oxygen, AICHE J. 64 (2018) 3958–3966, https://doi.org/10.1002/aic.16222.
[8] S.V. Nguyen, D. Dobuzinsky, D. Dopp, R. Gleason, M. Gibson, S. Fridmann, Plasma-Assisted Chemical Vapor Deposition and Characterization of High Quality Silicon Oxide Films, Thin Solid Films 194 (1990) 595–609, https://doi.org/10.1016/0040-6090(90)90211-U.
[9] C. Valle, A. Goullet, A. Granier, A. Van Der Lee, J. Durand, Inorganic to organic crossover in thin films deposited from O2/TEOS plasmas, J. Non-Cryst. Solids 272 (2000) 163–173.
[10] S.C. Deshmukh, E.S. Aydil, Investigation of SiO2 plasma enhanced chemical vapor deposition through tetraethoxysilane using attenuated total reflection Fourier transform infrared spectroscopy, J. Vac. Sci. Technol. A 13 (1995) 2355–2367, https://doi.org/10.1116/1.579521.
[11] K. Pfeiffer, S. Shestaeva, A. Bingel, P. Munzert, L. Ghazaryan, C. van Helvoirt, W.M.M. Kessels, U.T. Sanli, C. Grévent, G. Schütz, M. Putkonen, I. Buchanan, L. Jensen, D. Ristau, A. Tünnermann, A. Szeghalmi, Comparative study of ALD SiO2 thin films for optical applications, Opt. Mater. Express. 6 (2016) 660, https://doi.org/10.1364/OME.6.000660.
[12] V. Romero, V. Vega, J. García, R. Zierold, K. Nielsch, V.M. Prida, B. Hernando, J. Benavente, Changes in morphology and ionic transport induced by ALD SiO2 coating of nanoporous alumina membranes, ACS Appl. Mater. Interfaces 5 (2013) 3556–3564, https://doi.org/10.1021/am400300r.
[13] W.A. Pliskin, Comparison of properties of dielectric films deposited by various methods, J. Vac. Sci. Technol. 14 (1977) 1064–1081, https://doi.org/10.1116/1.569413.
[14] P.N. Sen, M.F. Thorpe, Phonons in AX2 glasses: from molecular to band-like modes, Phys. Rev. B 15 (1977) 4030–4038, https://doi.org/10.1103/PhysRevB.15.4030.
[15] F.L. Galeener, Band limits and the vibrational spectra of tetrahedral glasses, Phys. Rev. B 19 (1979) 4292–4297, https://doi.org/10.1103/PhysRevB.19.4292.
[16] S. Taraskin, S. Elliott, Nature of vibrational excitations in vitreous silica, Phys. Rev. B 56 (1997) 8605–8622, https://doi.org/10.1103/PhysRevB.56.8605.
[17] H. Schliwinski, U. Schnakenberg, W. Windbracke, F. Mikrostrukturtechnik, D. Berlin, Thermal Annealing Effects on the Mechanical Properties of Plasma-

Enhanced Chemical Vapor Deposited Silicon Oxide Films, 139 (2000), pp. 1730–1735.
[18] I. Montero, L. Galn, O. Najmi, J.M. Albella, Disorder-induced vibration-mode coupling in SiO2 films observed under normal-incidence infrared radiation, Phys. Rev. B 50 (1994) 4881–4884, https://doi.org/10.1103/PhysRevB.50.4881.
[19] P. Innocenzi, P. Falcaro, D. Grosso, F. Babonneau, Order disorder transitions and evolution of silica structure in self-assembled Mesostructured silica films studied through FTIR spectroscopy, J. Phys. Chem. B 107 (2003) 4711–4717, https://doi.org/10.1021/jp026609z.
[20] P. Lange, Evidence for disorder-induced vibrational mode coupling in thin amorphous SiO2 films, J. Appl. Phys. 66 (1989) 201–204, https://doi.org/10.1063/1.344472.
[21] C.T. Kirk, Quantitative analysis of the effect of disorder-induced mode coupling on infrared absorption in silica, Phys. Rev. B 38 (1988) 1255–1273.
[22] M.K. Gunde, Vibrational modes in amorphous silicon dioxide, Phys. B 292 (2000) 286–295, https://doi.org/10.1016/S0921-4526(00)00475-0.
[23] N. Primeau, C. Vautey, M. Langlet, The effect of thermal annealing on aerosol-gel deposited SiO2 films: a FTIR deconvolution study, Thin Solid Films 310 (1997) 47–56, https://doi.org/10.1016/S0040-6090(97)00340-4.
[24] F. Ruiz, J.R. Martınez, J. Gonzalez-Hernandez, A simple model to analyze vibrationally decoupled modes on SiO2 glasses, J. Mol. Struct. 641 (2002) 243–250, https://doi.org/10.1016/S0022-2860(02)00348-4.
[25] T.M. Parrill, Transmission infrared study of acid-catalyzed sol-gel silica coatings during room ambient drying, J. Mater. Res. 7 (1992) 2230–2239, https://doi.org/10.1557/JMR.1992.2230.
[26] P.G. Pai, S.S. Chao, Y. Takagi, G. Lucovsky, Infrared spectroscopic study of SiOx films produced by plasma enhanced chemical vapor deposition, J. Vac. Sci. Technol. 4 (1986) 689–694, https://doi.org/10.1116/1.573833.
[27] C. Charles, Characterization of silicon dioxide films deposited at low pressure and temperature in a helicon diffusion reactor, J. Vac. Sci. Technol. 11 (1993) 2954–2963, https://doi.org/10.1116/1.578675.
[28] A. Fidalgo, L.M. Ilharco, The defect structure of sol-gel-derived silica/polytetrahydrofuran hybrid films by FTIR, J. Non-Cryst. Solids 283 (2001) 144–154, https://doi.org/10.1016/S0022-3093(01)00418-5.
[29] D.V. Tsu, G. Lucovsky, B.N. Davidson, Effects of the nearest neighbors and the alloy matrix on SiH stretching vibrations in the amorphous SiOr:H (0 < r < 2) alloy system, Phys. Rev. B 40 (1989) 1795–1805, https://doi.org/10.1103/PhysRevB.40.1795.
[30] H. Yoshino, K. Kamiya, H. Nasu, IR study on the structural evolution of sol-gel derived SiO2 gels in the early stage of conversion to glasses, J. Non-Cryst. Solids 126 (1990) 68–78.
[31] C. Weigel, M. Foret, B. Hehlen, M. Kint, S. Clément, A. Polian, R. Vacher, B. Rufflé, Polarized Raman spectroscopy of v- SiO2 under rare-gas compression, Phys. Rev. B 93 (2016) 1–9, https://doi.org/10.1103/PhysRevB.93.224303.
[32] W. Pliskin, R. Gnall, Evidence for oxidation growth at the oxide-silicon Interface from controlled etch studies, J. Electrochem. Soc. 111 (1964) 872–873, https://doi.org/10.1149/1.2426271.
[33] C. Martinet, R.A.B. Devine, Analysis of the vibrational mode spectra of amorphous SiO2 films, J. Appl. Phys. 77 (1995) 4343–4348, https://doi.org/10.1063/1.359459.
[34] V. Rouessac, R. Coustel, F. Bosc, J. Durand, A. Ayral, Characterisation of mesostructured TiO2thin layers by ellipsometric porosimetry, Thin Solid Films 495 (2006) 232–236, https://doi.org/10.1016/j.tsf.2005.08.334.
[35] P. Revol, D. Perret, F. Bertin, F. Fusalba, V. Rouessac, A. Chabli, G. Passemard, A. Ayral, Porosimetry measurements on low dielectric constant-thin layers by coupling spectroscopic ellipsometry and solvent adsorption-desorption, J. Porous. Mater. 12 (2005) 113–121, https://doi.org/10.1007/s10934-005-6768-9.
[36] M. Mayer, SIMNRA User's Guide, Germany, (1997).
[37] I.W. Boyd, J.I.B. Wilson, A study of thin silicon dioxide films using infrared absorption techniques, J. Appl. Phys. 53 (1982) 4166–4172, https://doi.org/10.1063/1.331239.
[38] R.M. De Vos, W.F. Maier, H. Verweij, Hydrophobic silica membranes for gas separation, J. Memb. Sci. 158 (1999) 277–288, https://doi.org/10.1016/S0376-7388(99)00035-6.
[39] J. Gope, S. Kumar, S. Singh, C.M.S. Rauthan, P.C. Srivastava, Growth of mixed-phase amorphous and ultra nanocrystalline silicon thin films in the low pressure regime by a VHF PECVD process, Silicon. 4 (2012) 127–135, https://doi.org/10.1007/s12633-012-9109-z.
[40] L. He, Y. Kurata, T. Inokuma, S. Hasegawa, Analysis of SiH vibrational absorption in amorphous SiOx:H ($0 \le x \le 2.0$) alloys in terms of a charge-transfer model, Appl. Phys. Lett. 63 (1993) 162–164, https://doi.org/10.1063/1.110386.
[41] D. Rouchon, N. Rochat, F. Gustavo, A. Chabli, O. Renault, P. Besson, Study of ultrathin silicon oxide films by FTIR-ATR and ARXPS after wet chemical cleaning processes, Surf. Interface Anal. 34 (2002) 445–450, https://doi.org/10.1002/sia.1335.
[42] P. Innocenzi, Infrared spectroscopy of sol-gel derived silica-based films: a spectra-microstructure overview, J. Non-Cryst. Solids 316 (2003) 309–319, https://doi.org/10.1016/S0022-3093(02)01637-X.
[43] R.M. Almeida, H.C. Vasconcelos, L.M. Ilharco, Relationship between infrared absorption and porosity in silica-based sol-gel films, SPIE. 2288 (1994) 678–687, https://doi.org/10.1117/12.189004.
[44] J.T. Fitch, S.S. Kim, C.H. Bjorkman, G. Lucovsky, The effect of post-deposition thermal processing on MOS gate oxides formed by remote PECVD, J. Electron. Mater. 19 (1990) 151–158, https://doi.org/10.1007/BF02651740.
[45] S. Nguyen, D. Dobuzinsky, D. Harmon, S. Fridmann, Reaction Mechanisms of Plasma- and Thermal-Assisted Chemical Vapor deposition of Tetraethylorthosilicate Oxide Films, J. Electrochem. Soc. 137 (1990) 2209–2215, https://doi.org/10.1149/1.2086914.
[46] M.S. Haque, H.A. Naseem, W.D. Brown, Characterization of high rate deposited PECVD silicon dioxide films for MCM applications, J. Electrochem. Soc. 142 (1995) 3864–3869, https://doi.org/10.1149/1.2048425.
[47] T.M. Parrill, Heat treatment of spun-on acid-catalyzed sol-gel silica films, J. Mater. Res. 9 (1994) 723–730, https://doi.org/10.1557/JMR.1994.0723.
[48] Z. Yin, D.V. Tsu, G. Lucovsky, F.W. Smith, Annealing study of the infrared absorption in an amorphous silicon dioxide film, J. Non-Cryst. Solids 114 (1989) 459–461, https://doi.org/10.1016/0022-3093(89)90616-9.
[49] S.V. Nguyen, D. Dobuzinsky, D. Dopp, R. Gleason, M. Gibson, S. Fridmann, Plasma-assisted chemical vapor deposition and characterization of high quality silicon oxide films, Thin Solid Films 194 (1990) 595–609, https://doi.org/10.1016/0040-6090(90)90211-U.
[50] J.T. Fitch, Effects of thermal history on stress-related properties of very thin films of thermally grown silicon dioxide, J. Vac. Sci. Technol. B. 7 (1989) 153–162, https://doi.org/10.1116/1.584708.
[51] D. Davazoglou, V.E. Vamvakas, Optical dispersion analysis within the IR range of thermally grown and TEOS deposited SiO2 films, Microelectron. Reliab. 39 (1999) 285–289, https://doi.org/10.1016/S0026-2714(98)00217-0.
[52] D. Davazoglou, V.E. Vamvakas, Comparison of FTIR transmission spectra of thermally and LPCVD SiO2 films grown by TEOS pyrolysis, J. Electro. Soc. 151 (2004) 93–97, https://doi.org/10.1149/1.1676725.
[53] F.L. Galeener, Planar rings in glasses, Solid State Commun. 44 (1982) 1037–1040, https://doi.org/10.1016/0038-1098(82)90329-5.
[54] P. Lange, W. Windbracke, Characterization of thermal and deposited thin oxide layers by longitudinal optical-transverse optical excitation in fourier transform IR transmission measurements, Thin Solid Films 174 (1989) 159–164, https://doi.org/10.1016/0040-6090(89)90885-7.
[55] D.W. Berreman, Infrared absorption at longitudinal optic frequency in cubic crystal films, Phys. Rev. 130 (1963) 2193–2198, https://doi.org/10.1103/PhysRev.130.2193.
[56] B. Harbecke, B. Heinz, P. Grosse, Optical properties of thin films and the Berreman effect, Appl. Phys. A Solids Surfaces. 38 (1985) 263–267, https://doi.org/10.1007/BF00616061.
[57] N. Chemin, M. Klotz, V. Rouessac, A. Ayral, E. Barthel, Mechanical properties of mesoporous silica thin films: effect of the surfactant removal processes, Thin Solid Films 495 (2006) 210–213, https://doi.org/10.1016/j.tsf.2005.08.260.
[58] K. Hübner, L. Schumann, A. Lehmann, H.H. Vajen, G. Zuther, Detection of LO and TO phonons in amorphous SiO2 films by oblique incidence of IR light, Phys. Status Solidi 233 (1981) 301, https://doi.org/10.1002/pssb.2221040145.
[59] M. Putkonen, M. Bosund, O.M.E. Ylivaara, R.L. Puurunen, L. Kilpi, H. Ronkainen, S. Sintonen, S. Ali, H. Lipsanen, X. Liu, E. Haimi, S.P. Hannula, T. Sajavaara, I. Buchanan, E. Karwacki, M. Vähä-Nissi, Thermal and plasma enhanced atomic layer deposition of SiO2using commercial silicon precursors, Thin Solid Films 558 (2014) 93–98, https://doi.org/10.1016/j.tsf.2014.02.087.
[60] M. Creatore, S.M. Rieter, Y. Barrell, M.C.M. van de Sanden, R. Vernhes, L. Martinu, Optical and chemical characterization of expanding thermal plasma-deposited carbon-containing silicon dioxide-like films, Thin Solid Films 516 (2008) 8547–8553, https://doi.org/10.1016/j.tsf.2008.05.022.
[61] M.G.M. Van Der Vis, E. Cordfunke, R. Konings, The thermodynamic properties of tetraethoxysilane (TEOS) and an infrared study of its thermal decomposition, J. Phys. IV 03 (1993) 75–82, https://doi.org/10.1051/jp4:1993309.
[62] R. Etemadi, C. Godet, J. Perrin, A. Seignac, D. Ballutaud, Optical and compositional study of silicon oxide thin films deposited in a dual-mode (microwave/radio-frequency) plasma-enhanced chemical vapor deposition reactor, J. Appl. Phys. 83 (1998) 5224–5232, https://doi.org/10.1063/1.367343.
[63] W.S. Liao, S.C. Lee, Water-induced room-temperature oxidation of Si-H and -Si-Si-bonds in silicon oxide, J. Appl. Phys. 80 (1996) 1171–1176, https://doi.org/10.1063/1.362915.
[64] J.A. Theil, D.V. Tsu, G. Lucovsky, Reaction pathways and sources of OH groups in low temperature remote PECVD silicon dioxide thin films, J. Electron. Mater. 19 (1990) 209–217, https://doi.org/10.1007/BF02651747.
[65] Norio Hirashita, Shunichi Toikitoh, Hidetsugu Uchida, Thermal desorption and infrared studies of plasma-enhanced chemical vapor deposited SiO films with tetraethylorthosilicate, Jpn. J. Appl. Phys. 32 (1993) 1787–1793.
[66] C.J. Brinker, T.L. Ward, R. Sehgal, N.K. Raman, S.L. Hietala, D.M. Smith, D.W. Hua, T.J. Headley, “Ultramicroporous” silica-based supported inorganic membranes, J. Memb. Sci. 77 (1993) 165–179, https://doi.org/10.1016/0376-7388(93)85067-7.
[67] K. Shirono, H. Daiguji, Molecular simulation of the phase behavior of water confined in silica nanopores, J. Phys. Chem. C 111 (2007) 7938–7946, https://doi.org/10.1021/jp067380g.
[68] P.N.K. Deenapanray, Influence of low-temperature chemical vapor deposited SiO [sub 2] capping layer porosity on GaAs/AlGaAs quantum well intermixing, Electrochem. Solid-State Lett. 3 (2000) 196–199, https://doi.org/10.1149/1.1391000.
[69] G. Lucovsky, J.T. Fitch, E. Kobeda, E.A. Irene, Local atomic structure of thermally grown, Phys. Chem. (1988) 139–148 SiO2.
[70] C. Vallée, A. Goullet, F. Nicolazo, A. Granier, G. Turban, In situ ellipsometry and infrared analysis of PECVD SiO 2 films deposited in an O2/TEOS helicon reactor, J. Non-Cryst. Solids 216 (1997) 48–54.
[71] H. Juárez, M. Pacio, T. Díaz, E. Rosendo, G. Garcia, A. García, F. Mora, G. Escalante, Low temperature deposition: properties of SiO2 Tilms from TEOS and ozone by APCVD system, J. Phys. Conf. Ser. 167 (2009) 1–6, https://doi.org/10.1088/1742-6596/167/1/012020.